

Stable Obstacle Avoidance Strategy for Crawler-Type Intelligent Transportation Vehicle in Non-Structural Environment Based on Attention-Learning

Yitian Wang^{ID}, Jun Lin^{ID}, Liu Zhang, Tianhao Wang^{ID}, Member, IEEE, Hao Xu^{ID},
Yuehan Qi, Guanyu Zhang^{ID}, and Yang Liu^{ID}

Abstract—Existing intelligent driving technology often has difficulty balancing smooth driving and fast obstacle avoidance, especially when the vehicle is in a non-structural environment and is prone to instability during emergencies. Therefore, this study proposed an autonomous obstacle avoidance control strategy that can effectively guarantee vehicle stability based on an Attention-long short-term memory (Attention LSTM) deep learning model with the idea of humanoid driving. First, we designed the autonomous obstacle avoidance control rules to guarantee the safety of unmanned vehicles. Second, we improved the autonomous obstacle avoidance control strategy combined with the stability analysis of special vehicles. Third, we constructed a deep learning obstacle avoidance control based on the Attention-LSTM network model through experiments, and the average relative error of this system was 14.95%. Finally, the stability and accuracy of this control strategy were verified numerically and experimentally. The method proposed in this study can ensure that the unmanned vehicle can successfully avoid obstacles while driving smoothly.

Index Terms—Attention-LSTM, deep learning, intelligent vehicle, non-structural environment, obstacle avoidance strategy.

I. INTRODUCTION

WITH the acceleration of vehicle intelligentization, humanoid autonomous obstacle avoidance driving, an emerging technology in unmanned driving, has attracted more and more researchers [1], [2], [3], [4]. Among them, crawler-type intelligent transport vehicles are developed with increasingly essential functions and tasks, making them critical

Manuscript received 15 August 2022; revised 15 November 2022; accepted 30 November 2022. This work was supported in part by the Jilin Province Science and Technology Development Plan Project under Grant 20220201055G X; in part by the National Natural Science Foundation of China under Grant 41827803; and in part by the Science and Technology Development Project of Changchun, China, under Grant 21ZY21. The Associate Editor for this article was S. Mumtaz. (Corresponding authors: Guanyu Zhang; Yang Liu.)

Yitian Wang, Jun Lin, Liu Zhang, Tianhao Wang, Hao Xu, Guanyu Zhang, and Yang Liu are with the College of Instrumentation and Electrical Engineering, Jilin University, Changchun 130012, China (e-mail: yitian18@mails.jlu.edu.cn; lin_jun@jlu.edu.cn; zhangliu@jlu.edu.cn; wangtianhao@jlu.edu.cn; xuh20@mails.jlu.edu.cn; liu_yang@jlu.edu.cn).

Yuehan Qi is with the Department of Art and Science, Queen's University, Kingston, ON K7L 3N6, Canada (e-mail: 18yq36@queensu.ca).

Digital Object Identifier 10.1109/TITS.2022.3226493

equipment in special transport operations. However, they are often accompanied by safety hazards, such as collision and rollover during obstacle avoidance driving, since the working scenes of crawler-type intelligent transportation vehicles are mostly non-structural and complex environments, making it difficult to maintain the stability of the vehicle [5], [6]. Therefore, it is crucial to study how to improve the intelligent driving capability of crawler-type intelligent transport vehicles in non-structural environments.

For many years, various researchers have focused on crawler-type intelligent transportation vehicles. They have researched autonomous vehicle obstacle avoidance methods [7], [8], [9], [10], [11], [12], [13], [14], [15], [16], [17], [18]. Hu et al. proposed a path-planning method based on the off-road environment [19]. Schaub et al. introduced a two-stage clustering of the optical flow and proposed how those clusters can be used for obstacle evasion. Using this method, a simulation test was performed on the test site, and static and dynamic obstacles were successfully avoided [20]. Gim et al. proposed a new continuous curvature path generation method for poor comfort and low steering efficiency during vehicle obstacle avoidance lane change maneuvers [21]. Gla B. et al. proposed a risk assessment-based collision avoidance decision algorithm for multi-scene autonomous vehicles [22]. Li et al. proposed a method combining local trajectory planning and tracking control to solve the problem of vehicle lane changing and obstacle avoidance [23].

Deep learning methods can perform artificial intelligence tasks that require highly abstract features, such as image recognition and retrieval, natural language understanding. Deep learning methods have better scalability, robustness, and efficiency than traditional machine learning methods. Therefore, it is widely used in the field of assisted driving. In assisted driving, Shi et al. proposed a humanoid control method based on deep learning models to train driving data to predict braking decisions [24]. Chen et al. developed a vision-based deep Monte Carlo tree search (deep-MCTS) method for automatic driving control, which can predict driving behavior and help improve driving control stability and performance [25]. Sun et al. proposed a fuzzy algorithm-based driver- driving behavior

classification method and established a brain-based decision linear neural networks to implement humanoid driving [26]. Liang et al. proposed a target detection algorithm based on machine vision and neural network to improve the safety of autonomous driving [27]. Liu et al. applied the neural network module to the three-dimensional target detection of automatic driving, which improved the prediction performance of the system [28]. Aladem et al. proposed a single-stream dual-task network that performed semantic segmentation and monocular depth without using multiple decoders, improving the system performance of self-driving vision perception [29]. Huang et al. proposed a prediction model based on LSTM neural network to capture real traffic flow features by introducing human driving memory [30]. Zhang et al. proposed a new MV-CNN model for training and recognition of driving behavior by learning sample data collected from in-vehicle sensors [31].

However, the control effect of driving behavior in the above studies is far from that of human drivers as human drivers perceive more knowledge, such as vehicle status and environmental information, while driving a vehicle. This influences the human driver's operational intention and improves the driver's driving habits. Therefore, we choose to learn the driving habits of human drivers for better control and to reduce accidents.

In summary, we constructed a humanoid driving model based on deep learning. First, a stable obstacle avoidance control strategy based on deep learning is proposed. Second, a training data set is established using a virtual prototype. Finally, the accuracy of the method is verified through simulation and experiment. The experimental results show that the method has good accuracy and stability.

Compared with the existing work, the main contributions of this study lie in the following three aspects:

(1) Combined with the driving habits of human drivers, a method is proposed to classify obstacles based on their characteristics and spatial location, which helps to plan the best obstacle avoidance path for vehicles.

(2) An evaluation index for the driving stability of crawler-type intelligent transportation vehicles based on non-structural roads is proposed, which can guide the development of control algorithms for these vehicles.

(3) An obstacle avoidance control strategy that combines the idea of humanoid driving is proposed. The strategy enables the crawler-type intelligent transporter to independently accomplish stable obstacle avoidance behavior when encountering obstacles in a non-structural slope environment.

II. PROBLEM DESCRIPTION

The crawler-type intelligent transportation vehicle has a high center of gravity. Further, the field environment where the vehicle works is mostly in mountainous areas with a slope greater than 5° , as shown in Figure 1. The vehicle will generate a large lateral acceleration when the crawler-type intelligent transportation vehicle is in an emergency obstacle avoidance and turning state. The road is rough because of many trees, wild rocks, and other obstacles on the hillside. The



Fig. 1. Example of actual working scene of crawler-type vehicles. (a) Mountain scene; (b) Field scene; (c) Desert scene; (d) Snow scene.

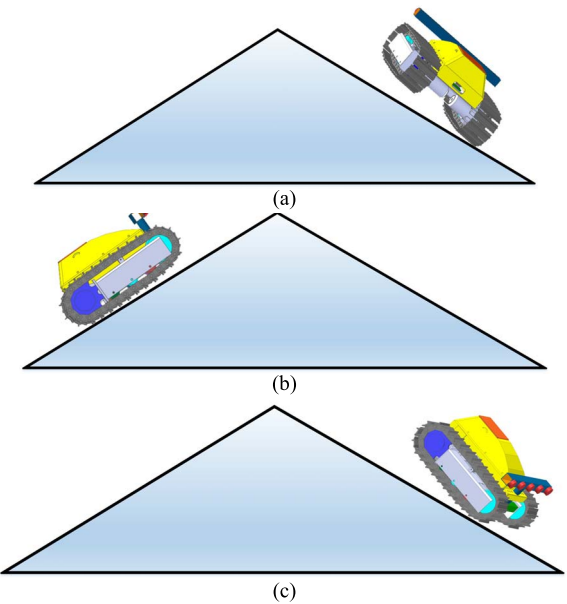


Fig. 2. Schematic diagram of instability of crawler-type intelligent transport vehicle. (a) Steering and tipping; (b) Longitudinal uphill tipping; (c) Longitudinal downhill tipping.

vehicle will continue crossing undulating obstacles during the driving process, resulting in aggravated instability [32], [33], [34], [35].

The tipping situation is as follows:

a. Steering and tipping: When the vehicle is driving on a slope with a slope angle of β , the lateral acceleration of the vehicle is not zero due to the action of the ground gravity, the supporting force and the friction force of the slope, and the critical angular velocity of rollover changes, and the vehicle is prone to rollover, as shown in Fig. 2(a).

b. Longitudinal uphill tipping: Crawler-type intelligent transportation vehicles in the longitudinal uphill turning and obstacle avoidance process due to the increase in the slope angle makes the vehicle along the slope direction of the component force increases, making the vehicle produce along

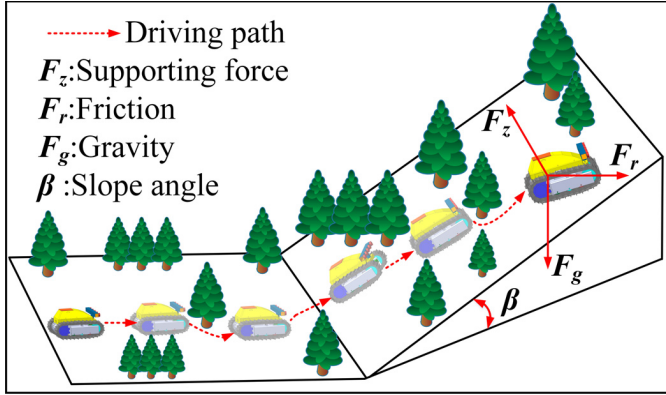


Fig. 3. Schematic diagram of the vehicle obstacle avoidance process based on a non-structural road.

the slope face downward side tilt angle, resulting in the vehicle under the slope when the side tilt angle increases, as shown in Fig. 2(b).

c. Longitudinal downhill tipping: When the crawler-type intelligent transportation vehicle is in the longitudinal downhill turning and obstacle avoidance process, the component force of the vehicle along the slope direction decrease due to the decrease of slope angle, making the vehicle produce the side inclination angle along the slope facing upward, increasing of the side inclination angle when the vehicle is under the slope, as shown in Fig. 2(c).

As shown in Figure 3, it is difficult for unmanned vehicles to plan a stable and smooth obstacle avoidance path in the process of obstacle avoidance as professional drivers do due to the highly complex working environment and operational requirements of crawler-type intelligent transportation vehicles, which has a significant impact on the safety and stability of unmanned vehicles. Thus, we proposed an active control strategy to adjust the vehicle posture and improve the stability of vehicle obstacle avoidance.

III. METHOD

First, we constructed an obstacle information detection system and proposed an obstacle classification strategy based on obstacle characteristics and spatial relative position relationship to classify the obstacles ahead into 15 situations. Second, we analyzed the stability index threshold of the vehicle under the limit state. Finally, we adjusted the vehicle driving control strategy under the current emergency based on the location and state information of the obstacles and vehicles, respectively, as the input of the deep learning model.

A. Obstacle Avoidance Strategy

1) *Analysis of Spatial Relative Position Relationship of Detection Target:* Ultrasonic sensors use high-frequency sound waves to detect the position and distance of objects with strong directionality and can be used to obtain obstacle information about the surrounding environment. A proper sensor layout can effectively reduce the blind spot of obstacle perception. Therefore, in this study, we constructed an obstacle information detection system based on the ultrasonic sensor.

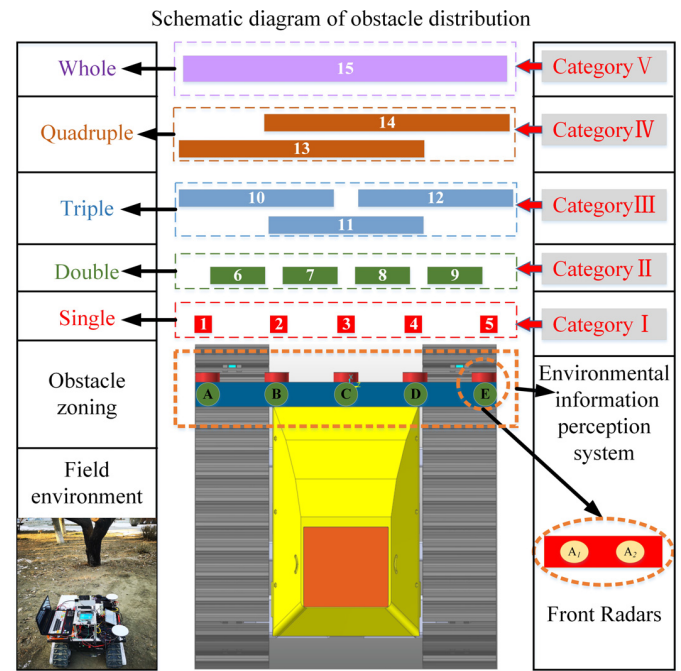


Fig. 4. Schematic diagram of the field obstacle classification based on obstacle information detection system.

In engineering applications, it is necessary to ensure the successful obstacle avoidance of vehicles and the easy realization of the design of the decision planning. The crawler-type intelligent transport vehicles need to use the obstacle information detection system to autonomously classify field obstacles due to the complex field environment, harsh working conditions, and no apparent marking guidelines and traffic signals on non-structural roads. Therefore, we proposed an obstacle classification strategy based on obstacle characteristics and spatial relative position relationships. First, the ultrasonic sensor in front of the vehicle head must detect the position and size of the obstacles in the front. Second, we formulated the corresponding obstacle avoidance rules for different obstacles. Considering the continuity of obstacles, we divided the obstacles into five categories based on the location and size of obstacles in the field, as shown in Fig. 4. The five categories are as follows:

I: The vehicle adjusts its heading angle according to the obstacle's position at this time when the obstacle at the scene is detected by only one group of the ultrasonic range radar, as shown in cases 1–5 in Fig. 4.

II: The vehicle adjusts its heading angle according to the obstacle's position at this time when the obstacle at the scene is detected only by two sets of the ultrasonic range radar, as shown in cases 6–9 in Fig. 4.

III: The vehicle adjusts its heading angle according to the obstacle's position at this time when the obstacle at the scene is detected by three sets of the ultrasonic range radar, as shown in cases 10–12 in Fig. 4.

IV: The vehicle adjusts its heading angle according to the obstacle's position when an obstacle at the site is detected by four sets of the ultrasonic ranging radar, as shown in cases 13 and 14 in Fig. 4.

V: The vehicle adjusts its heading angle according to the obstacle's position at this time when the obstacle at the site is detected by five sets of ultrasonic range radar, as shown in case 15 in Fig. 4.

2) Obstacle Avoidance Rule Design: According to the requirement that the crawler-type intelligent transportation vehicle needs to maintain stable driving on non-structural roads, the vehicle dynamics constraints and the stability constraints in the obstacle avoidance process are comprehensively considered, and the vehicle lateral and longitudinal speed controls are combined for steering control. There are multiple avoidance paths when the vehicle encounters an obstacle. The vehicle not only needs to turn and avoid based on the direction of the obstacle but also decelerate along the tangent direction of the obstacle. In the process of vehicle driving, according to engineering requirements, both sides of the vehicle should be reserved a certain safety distance q (q value should always be greater than 200 mm) to ensure that the vehicle can safely avoid obstacles. Fig. 5 shows the expert obstacle avoidance path process for crawler-type intelligent transport vehicles. The vehicle speed is regulated by the track speed v_l and v_r on the left and right sides, where the red dot is the current target point. When the crawler-type intelligent transport vehicle is driving on the road in the wild, the obstacle information detection system of the vehicle starts to work, and the shaded area in front is the monitoring area. In contrast, the crawler-type intelligent transport vehicle maintains the original heading and drives to the target point when the vehicle-mounted radar does not detect the obstacle. When the vehicle-mounted radar detects the obstacle ahead, the vehicle adjusts its direction to turn left or right to avoid the obstacle. The size of the steering angle θ_m is related to the position of the obstacle.

The unmanned vehicle's forward and steering angular velocities at moment t can be expressed as [36], [37], and [38]:

$$\begin{cases} \dot{x}(t) = \frac{1}{2}(v_l + v_r) \cos \theta_d \\ \dot{y}(t) = \frac{1}{2}(v_l + v_r) \sin \theta_d \\ \dot{\theta}_d(t) = \frac{-v_l + v_r}{D + 2b} \end{cases} \quad (1)$$

where, v_l and v_r are the linear speed of the tracks on the left and right sides of the crawler vehicle, respectively, D is the body width of the crawler vehicle, b is the track width, and θ_d is the heading angle of the vehicle, as shown in Figure 5.

Then, the equation of the state of motion of the unmanned vehicle can be expressed as follows:

$$\begin{aligned} \dot{W} &= \begin{bmatrix} \dot{x} \\ \dot{y} \\ \dot{\theta}_d \end{bmatrix} = \begin{bmatrix} \cos \theta_d & 0 \\ \sin \theta_d & 0 \\ 0 & 1 \end{bmatrix} \begin{bmatrix} v_o \\ \omega_o \end{bmatrix} \\ &= \begin{bmatrix} \frac{1}{2} \cos \theta_d & \frac{1}{2} \cos \theta_d \\ \frac{1}{2} \sin \theta_d & \frac{1}{2} \sin \theta_d \\ -\frac{1}{D+2b} & \frac{1}{D+2b} \end{bmatrix} \begin{bmatrix} v_l \\ v_r \end{bmatrix} \end{aligned} \quad (2)$$

The turning radius R of the track is given by

$$R = \frac{(2v_r + \Delta v)(D + 2b)}{2\Delta v} \quad (3)$$

The heading angle of the unmanned vehicle can be calculated using Eq. (4), where $i = 1, 2, \dots, 5$ and $m = 1, 2, \dots, 15$.

$$\theta_m = \arctan \frac{q + R_i}{1500} \quad (4)$$

In order to give the vehicle more space to avoid obstacles in the obstacle avoidance process, we set 1500mm as the warning distance of the vehicle based on the factors of track chassis length and speed. When the distance between the front obstacle and the vehicle head reaches 1500mm, the vehicle starts to process the obstacle signal.

Formula (4) for the vehicle's steering angle formula: $q + R_i$ the physical significance of the front obstacle from the center of the head of the transverse distance, 1500mm for the longitudinal distance of the obstacle from the front of the vehicle, from which you can calculate the steering angle required to avoid the obstacle.

After calculating the above formula, reserving a certain safety margin for the steering angle of the crawler-type intelligent transport vehicle, and considering various engineering factors, the actual steering angle of the unmanned vehicle can be determined. Table I lists the calculation results of θ_m .

θ_m is the actual steering angle of the crawler-type intelligent transportation vehicle for obstacle avoidance, “-” means it turns right, “+” means it turns left, ω_s ($\omega_s = 5.5$ rad/s) is the initial drive wheel speed of both sides during the straight running condition, v_s ($v_s = 0.9$ m/s) is the initial linear velocity of the vehicle, ω_L and ω_R are the rotational speeds of the left and right track driving wheels, respectively, and ω_o linear velocity of the geometric center point of the vehicle track. To sum up, the flow of vehicle autonomous obstacle avoidance algorithm based on the non-structural road is shown in algorithm I.

B. Vehicle Stability Monitoring

This study must analyze and evaluate the dynamic stability of the vehicle to improve the driving stability of the vehicle. Dynamic stability is an important criterion for evaluating vehicle stability. A vehicle is judged to be stable through the analysis of stability indicators, and then early warning and active anti-roll control strategy are implemented. There are various reasons for the vehicle's instability, such as climbing and rolling over, road collapse, side slip and tripping, and fast turning when encountering obstacles. Regardless of the vehicle instability's cause, there must be some standard features before it. The features include the lateral acceleration of the vehicle, transverse angular acceleration, lateral angular velocity, lateral tilt angle, and other parameters that have exceeded a specific threshold value. Therefore, in this study, we employed an inertial measurement unit (IMU) to collect vehicle state parameters, such as three-axis attitude angle, three-axis angular velocity, and centroid dynamics during driving.

A certain safety distance margin must be maintained between the vehicle and the obstacle's edge. At the same time,

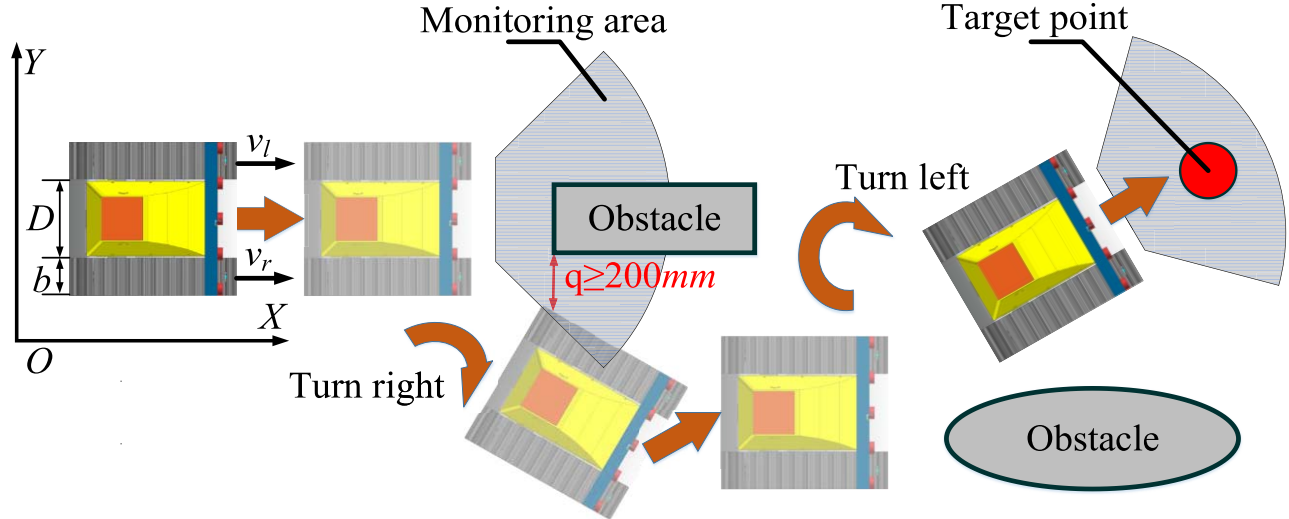


Fig. 5. Schematic diagram of the obstacle avoidance path of the crawler-type intelligent transport vehicle.

TABLE I
OBSTACLE AVOIDANCE STRATEGIES FOR OBSTACLES IN DIFFERENT LOCATIONS

Condition	A	B	C	D	E	$\theta_m (\circ)$	$\omega_l (\text{rad/s})$	$\omega_r (\text{rad/s})$	$\omega_o (\text{rad/s})$
1	1	0	0	0	0	-6	1.5	0.5	1
2	0	1	0	0	0	-20	4.5	1.6	3.05
3	0	0	1	0	0	-28	6.8	2.4	4.6
4	0	0	0	1	0	+20	1.6	4.5	3.05
5	0	0	0	0	1	+6	0.5	1.5	1
6	1	1	0	0	0	-20	4.5	1.6	3.05
7	0	1	1	0	0	-28	6.8	2.4	4.6
8	0	0	1	1	0	+28	2.4	6.8	4.6
9	0	0	0	1	1	+20	1.6	4.5	3.05
10	1	1	1	0	0	-28	6.8	2.4	4.6
11	0	1	1	1	0	-45	10.8	3.9	7.35
12	0	0	1	1	1	+28	2.4	6.8	4.6
13	1	1	1	1	0	-42	10	3.6	6.8
14	0	1	1	1	1	+42	3.6	10	6.8
15	1	1	1	1	1	-65	15.6	5.2	10.6

other suboptimal paths have long distances and too many sharp turns, resulting in a significant yaw rate acceleration and poor stability. Therefore, our proposed stability control rule aims to find the best path to avoid obstacles while maintaining body stability. Based on the slope information and the driving information of the vehicle itself, the dynamic stability index of crawler-type intelligent transportation vehicle can be expressed as [39], and [40]:

$$DSE_{\min} = \frac{\beta}{\beta_{\max}} \lambda \cdot \{a_x, a_y, a_z, a_{rx}, a_{ry}, a_{rz}\}^T \quad (5)$$

In Eq. (5), β_{\max} is the maximum road climbing angle of the crawler-type intelligent transport vehicle, a_x , a_y , and a_z are the lateral acceleration, forward acceleration, and longitudinal acceleration of the crawler-type intelligent transport vehicle, respectively, a_{rz} , a_{ry} , and a_{rx} are the pitch angle acceleration, roll angle acceleration, and heading angle acceleration of the crawler-type intelligent transport vehicle, respectively. This evaluation index integrates the vehicle motion parameters and road slope angle. In addition, λ Is the weight vector.

Through our experiments, we have obtained the vehicle's forward, lateral, heading angular, pitch angle, and roll angular

TABLE II
INSTABILITY EVALUATION INDEX TABLE OF CRAWLER-TYPE INTELLIGENT TRANSPORTATION VEHICLE

Evaluating indicator	Values	Units
a_x	≤ 1	g
a_y	≤ 0.8	g
a_z	≤ 2	g
a_{rx}	≤ 9	rad/s ²
a_{ry}	≤ 13	rad/s ²
a_{rz}	≤ 16	rad/s ²
β	≤ 20	°
DSE (max)	7.26	-

accelerations, which will significantly impact the driving stability of the crawler-type intelligent transport vehicle.

The vehicle's lateral and forward acceleration, lateral pitch angular velocity, and heading angular velocity play a decisive role in the vehicle's driving stability when the vehicle is driven on a non-structural road. The longitudinal acceleration and pitch angular velocity have less influence on the driving stability, and the results indicate that the influence of the former ones is about two times of the latter; therefore, we determine the weight vector λ in this study as $\{0.2, 0.2, 0.1, 0.1, 0.5, 0.6\}$. Table II lists the stability index constraints.

This study used Attention-long short-term memory (Attention-LSTM) based on the deep learning method to adjust the driving control strategy of the vehicle based on the processed obstacle information and vehicle driving data and ensure driving stability during obstacle avoidance.

C. Improved Attention-LSTM Model for Vehicle Control Strategy

It is necessary to use the obstacle information detection system to process and analyze the obstacle information in real-time due to the relatively complex environment of non-structural roads. Considering that the vehicle central control unit has no reference track and off-line map, it is difficult to make various expert experience judgments on obstacles.

Deep learning has powerful complex system characterization capability, big data processing capability, and automatic feature extraction capability, which is feasible and superior in detection tasks. Based on these, this study proposed a multi-level obstacle avoidance prediction network model, which is based on LSTM (long short-term memory) model and encoder-decoder structure [41], [42], [43]. A multi-level obstacle avoidance mechanism was introduced to model the dynamic spatiotemporal correlation between the sensors of the unmanned crawler vehicle to address the problem of high-stability obstacle avoidance.

Based on the recurrent neural network (RNN) model, LSTM adds an input gate, forgetting gate, output gate, and cell unit, as shown in Fig. 6. Among them, three control gates are responsible for controlling the inflow and outflow of information. Thus, protecting and controlling the cell unit's state is responsible for remembering the information of the previous

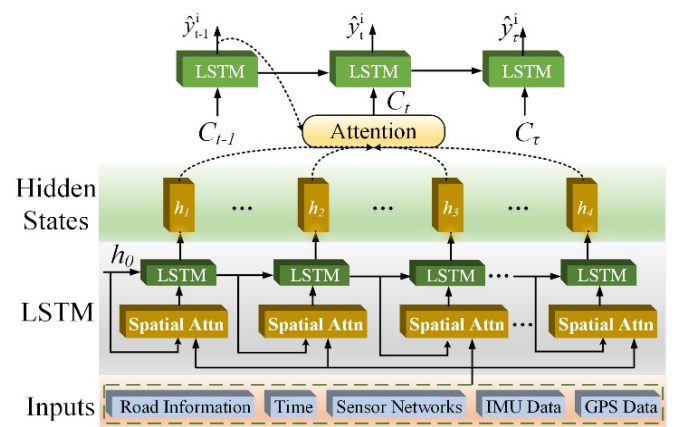


Fig. 6. Structure diagram of multi-level obstacle avoidance network model based on attention mechanism.

moment. From Fig. 6, the forward propagation formula of the LSTM unit can be deduced as follows:

$$f_t = \sigma(W_f \cdot [h_{t-1}, x_t] + b_f) \quad (6)$$

where W_f is the weight, b_f is the bias, σ is the sigmoid activation function, x_t is the current input value, and h_{t-1} is the output value of the upper hidden layer at the last moment.

Then, the model generates new update information, and this step consists of two parts:

(1) The input layer determines which values to use for the update by using the sigmoid activation function and noting the updated value;

(2) The new memory cell candidates are generated using the activation function $tanh$; then, combine the generated values from these two parts to update:

$$i_t = \sigma(W_i \cdot [h_{t-1}, x_t] + b_i) \quad (7)$$

$$\tilde{C}_t = \tanh(W_C \cdot [h_{t-1}, x_t] + b_C) \quad (8)$$

where W_i is the weight of the updated value, b_i is the bias of the updated value, \tilde{C}_t is the candidate value of the memory cell, W_C is the weight of the updated value, and b_C is the bias of the updated value.

Subsequently, the old memory cells will be updated:

$$C_t = f_t * C_{t-1} + i_t * \tilde{C}_t \quad (9)$$

Algorithm 1 The Algorithm Flow of the Vehicle Autonomous Obstacle Avoidance Control Based on Non-Structural Road

```

Initialize environment settings (vehicle and obstacles);
Set safe obstacle avoidance distance for vehicles
 $L_T = 1500mm;$ 
Data Set:  $I_S$  (As shown in Section III A 1)
Input:Obstacle information and vehicle status parameters
Output: Heading angle and vehicle speed
1. Determine the three-dimensional coordinates of the target point ( $x, y, z$ );
2. Crawler-type intelligent transport vehicle starts driving;
3. Record the detection data of the ultrasonic sensor;
4. Multi-sensor information fusion;
5. foreach  $i [A, B, \dots, E]$  do
6.    $L_i \leftarrow$ Ranging value of each group of ultrasonic radar sensors (after fusion);
7.   if  $L_i \leq L_T$  then
8.     step1: Classify obstacles (Figure 4);
9.     step2: Adjust the speed of the tracks on both sides ( $\omega_L, \omega_R$ ) according to the obstacle avoidance strategy in Table I;
10.    step3: Drive at speed vs to avoid obstacles;
11.    step4: Vehicle returns to the initial course;
12.  else
13.    Keep the original course and drive to the target point;
14.  end
15.  Keep driving;
16.  if  $L_i \leq L_T$  then
17.    Continue to implement the above obstacle avoidance strategy;
18.  else
19.    Continue driving to the target point;
20.  end
21. end
22. The vehicle continues to the target point;
23. Using the system to collect operation data and experience.

```

The last step is to determine the output of the model. Firstly, the initial output is obtained through the sigmoid layer; secondly, its value is scaled between -1 and 1 using $tanh$, then it is multiplied one by one with the output obtained from the sigmoid, and finally, the output of the model is obtained.

$$o_t = \sigma (W_o [h_{t-1}, x_t] + b_o) \quad (10)$$

$$h_t = o_t * \tanh(C_t) \quad (11)$$

where W_o is the weight of the output value, b_o is the bias of the output value, o_t is the current output value, h_t is the current output state value of the hidden layer.

LSTM can save historical information, inheriting the traditional neural network's advantages and excavating historical time data [44], [45], [46], [47], [48], [49], [50], [51], [52]. The traditional LSTM converts the input sequence into a fixed length vector and saves all the information, limiting the model memory, and it is easy to lose information when dealing with long sequence problems. A single LSTM model converts the input sequence into a fixed-length vector and saves all the information. Moreover, it cannot detect the essential parts that affect the current obstacle avoidance strategy, reducing the utilization of information. In this study, the vehicle's excessive rolling angular and lateral acceleration can cause vehicle instability, according to the experience. The addition of an attention mechanism can make up for this defect. It can give weight to different information and strengthen the memory of important information. This study combines LSTM with the attention mechanism for high-stability obstacle avoidance strategy prediction. The overall structure of the Attention-LSTM prediction model proposed in this study is shown in Fig. 6.

D. Design of Stability Obstacle Avoidance Control Framework

This study proposed a stabilization and obstacle avoidance control strategy based on deep learning modeling using the Attention-LSTM deep learning method to realize the dynamic prediction of vehicle stabilization and obstacle avoidance strategy under the harsh environment in the field. Fig. 6 shows the schematic diagram of the control strategy, and the framework consists of three parts.

Part I: Vehicle obstacle avoidance strategy. We developed the corresponding expert bypass strategy based on different obstacle information to find the optimal safe path to avoid the obstacles ahead under the condition of the shortest path. First, an obstacle classification strategy was proposed based on obstacle characteristics and spatial relative position relationships. The obstacle information perception system was used to obtain the obstacle information in front. Second, an optimal obstacle avoidance strategy was designed to avoid obstacles on the vehicle route. Unmanned vehicles avoid collision between vehicles and obstacles by automatically adjusting the driving attitude of vehicles. The vehicle obstacle avoidance strategy is shown in part I of Fig. 7.

Part II: Vehicle stability judgment. First, the vehicle used IMU to collect the motion state information during driving (including three-axis attitude angle, three-axis angular velocity, and centroid position), in which the vehicle pitch angle collected by IMU can be used to calculate the slope angle of the current slope. Subsequently, the vehicle's dynamic stability was summarized and analyzed by comparing the changes in various parameters during vehicle driving. The vehicle stability judgment is shown in part II of Fig. 7.

Part III: Learn expert obstacle avoidance strategies. To find the optimal safe path to avoid the obstacles ahead under the condition of the shortest path, this study developed the corresponding expert bypassing strategy based on different obstacle information. It used Attention-LSTM to adjust the

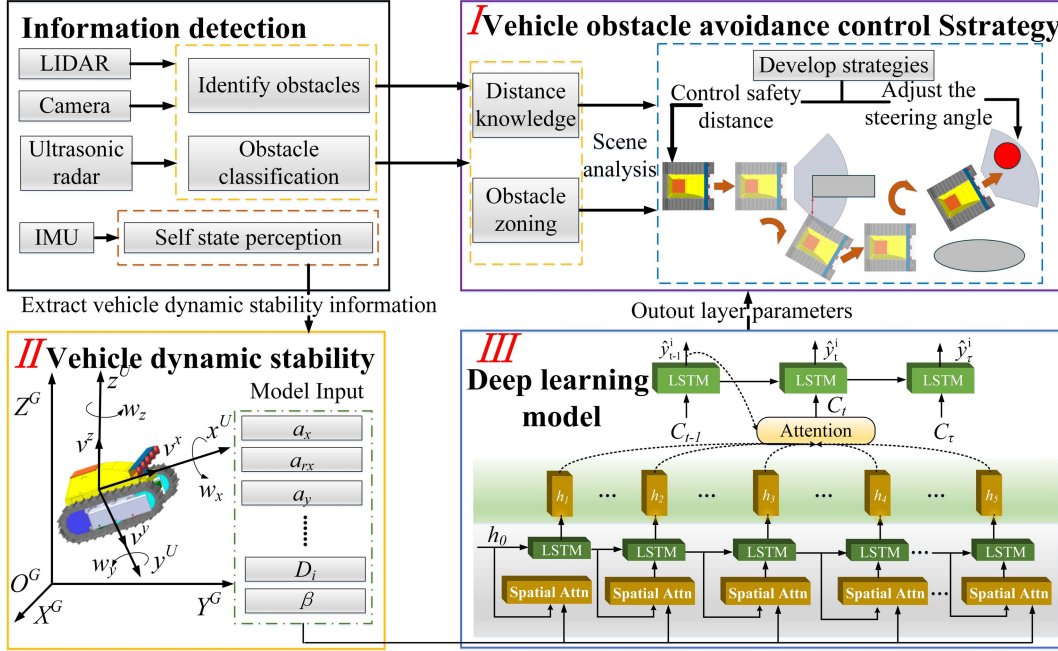


Fig. 7. Design of stability obstacle avoidance control strategy framework.

optimal obstacle avoidance strategy of the vehicle based on the processed obstacle information and vehicle driving data. Attention-LSTM is a new recurrent neural network structure based on a gradient learning algorithm, which solves the problem of gradient disappearance and gradient explosion during the training of long sequences. This structure has certain advantages in sequence modeling and has a long-term memory function, which will be applied in this study. This strategy has the features of simple logic and easy implementation. In this study, we used this feature to predict the obstacle avoidance strategy of crawler-type intelligent transportation vehicles. Learn expert obstacle avoidance strategies are shown in part in Fig. 7.

IV. SIMULATION AND EXPERIMENT

Deep learning has been successfully applied to many engineering fields. A common feature of these applications is the need to use large amounts of feature data to train deep-learning models. The working environment of crawler-type intelligent transport vehicles is relatively harsh, and the instability conditions are relatively complex in field experiments. However, it is not an economical and practical method to wear the crawler-type intelligent transportation vehicle only to verify the obstacle avoidance control strategy. Therefore, we used virtual prototype simulation to establish the data set. The effectiveness of this method needs to be fully verified in simulation experiments before large-scale field experiments can be carried out.

A. Simulation Settings

The speed and heading angle of the crawler-type intelligent transport vehicle are planned in real-time by the central computing unit, as shown in Fig. 8. We used a virtual

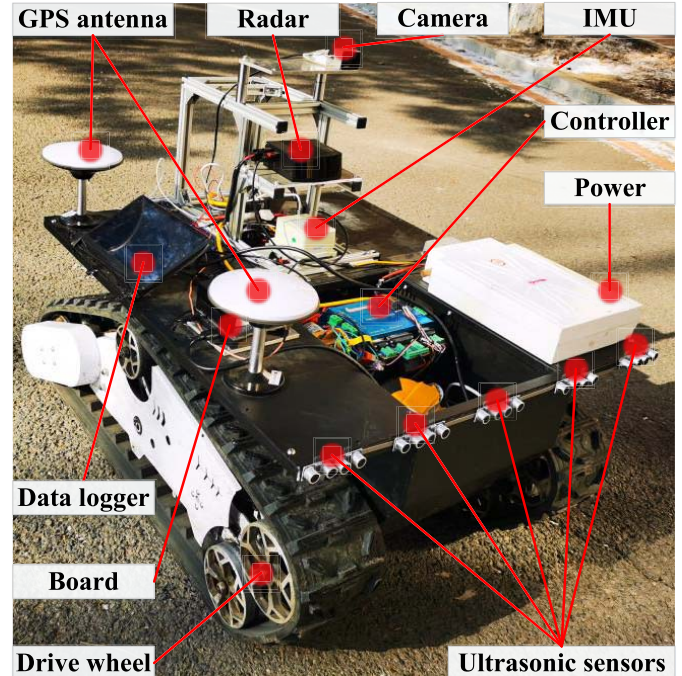


Fig. 8. Structural diagram of crawler-type intelligent transport vehicle.

prototype model to acquire data sets based on the relevant design parameters of the crawler-type intelligent transportation vehicle since dangerous situations, such as vehicle rollover, may occur during the experiment. Then, we conducted ground experiments to verify the effectiveness and stability of the method.

The relevant technical parameters of the crawler-type intelligent transport vehicle designed in this study are shown in Table III.

TABLE III
DESIGN PARAMETERS OF UNMANNED VEHICLE CHASSIS FOR TEST

Symbol	Parameter	Values	Units	Symbol	Parameter	Values	Units
m	Chassis quality	450	Kg	R_c	Driven wheel radius	0.14	m
b	Gauge	1	m	R_z	Radius of supporting wheel	0.13	m
D	Body width	1.25	m	V_{max}	Maximum travel speed	2.8	m/s
L_t	Total length of crawler chassis	1.2	m	i	Reduction ratio	100	m
l	Crawler ground length	0.881	m	T	Main traction force	500	Kg
H	Crawler height	0.331	m	β	Maximum climbing angle	30	Angle
R_d	Drive wheel radius	0.17	m	P	Ground pressure	0.045	Mpa

TABLE IV
GROUND CONTACT PARAMETER SETTING

Parameter	Values
Terrain Stiffness	4.7613e-004
Cohesion	1.04e-003
Shearing Resistance Angle	28
Shearing Deformation Modulus	25
Sinkage Ratio	5.e-002

B. Simulation Experiment

In this section, we used the vehicle dynamics software RecurDyn and the simulation software Matlab/Simulink for joint simulation, the establishment of the driving control model of crawler-type intelligent transportation vehicle in Simulink, and the development of the kinematics and dynamics model in RecurDyn. According to the above design requirements, the Matlab/Simulink-RecurDyn joint simulation model of the active control system combined with the idea of human-like driving is shown in Fig. 9. First, an obstacle information perception system is used in the environment information perception layer to obtain the current environment information. Second, an IMU is used in the vehicle state information perception layer to sense the real-time changes of vehicle state; then, the fused information is input into the Attention-LSTM network according to the human driving thoughts; finally, the best driving behavior under the current working conditions is obtained.

We referred to relevant literature and set the following ground contact parameters, as shown in Table IV, to better analyze the driving process of unmanned vehicles.

C. Establishment of Data Set

A virtual prototype was used to learn the driving habits of human drivers for joint simulation to obtain the training data set. We preset 15 kinds of obstacles in the simulation environment and conducted simulation experiments according to different slope conditions and obstacle distributions. In this section, 500 simulation experiments were performed and 5000 sets of valid data were selected for training (each set contains vehicle motion state parameters and corresponding sensor data). In building the anthropomorphic driving network,

the operator of the remote control vehicle driving has obtained the “Special equipment operator’s certificate,” and compared with other operators, the control operation of this operator is more skilled and has good experience in operating special equipment. Fig. 10 shows obstacle avoidance conditions and the vehicle’s three-axis attitude angle data. Among them, (a) is the obstacle avoidance condition of the unmanned vehicle on the flat road; (b) is the obstacle avoidance condition of the unmanned vehicle climbing; (c) is the obstacle avoidance condition of the unmanned vehicle downhill; (d) is the obstacle avoidance condition of the unmanned vehicle longitudinal slope. From Fig. 10, the sensor data changes relatively smoothly, and the current slope information can be obtained using the roll and pitch angles of the unmanned vehicle. The collected vehicle data include obstacle distribution, climbing angle, three-axis attitude angle, the dynamic position of the mass center, three-axis acceleration, and speed of the crawler driving wheels on both sides. The location information of the obstacles and the state information of the vehicle is set as the inputs to the prediction model to provide training data.

V. RESULTS AND DISCUSSION

A. Results of Attention-LSTM and Comparison With Other Models

According to the input of different ground slope information, we divided obstacle avoidance conditions into two types: based on uphill and downhill obstacle avoidance and longitudinal slope obstacle avoidance, and two deep learning networks were trained. In this study, we set the initial learning rate to 0.005, batch size to 20, and Maxepochs to 2000. RMSE and loss during training are shown in Fig. 11. For ease of understanding, the coordinates of RMSE (right ordinate) increase from top to bottom since both RMSE and loss decrease with the increase of iteration times. The RMSE has reached a relatively low level in a short time. The results show no overfitting or underfitting phenomenon in the network, which shows that the model has good generalization ability.

Based on Fig. 12, the RMSE and average relative error rate of the model gradually decrease as the slope decreases, indicating that the regression performance of the model improves as the slope decreases. The maximum average relative error rate reaches 19.3% when the slope is 15°, possibly due to the rapid change of driving information and complex

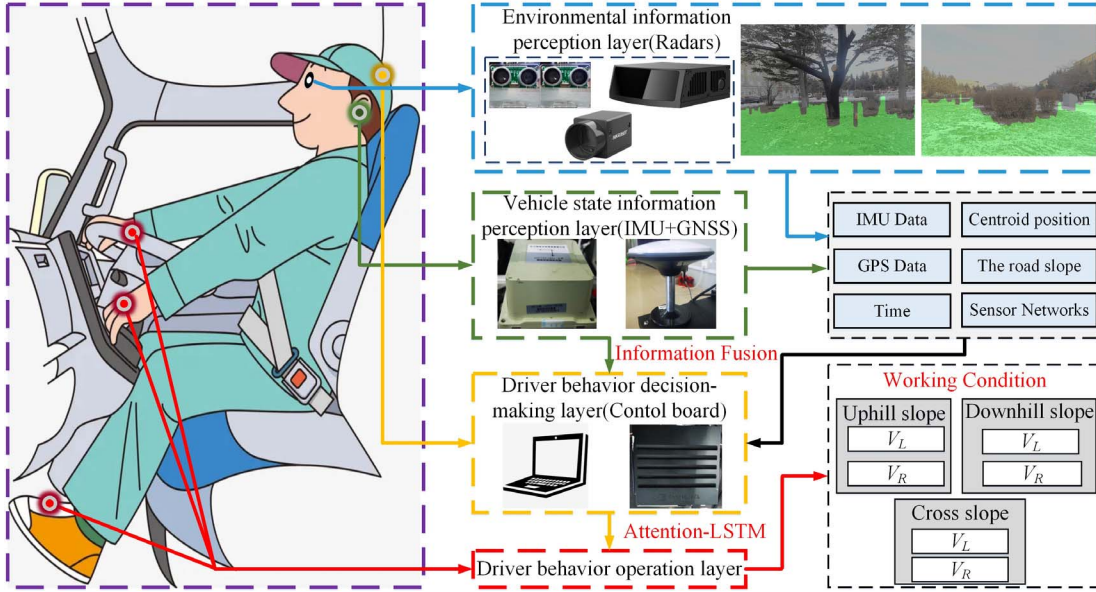


Fig. 9. Composition diagram of the active control system combined with human-like driving.

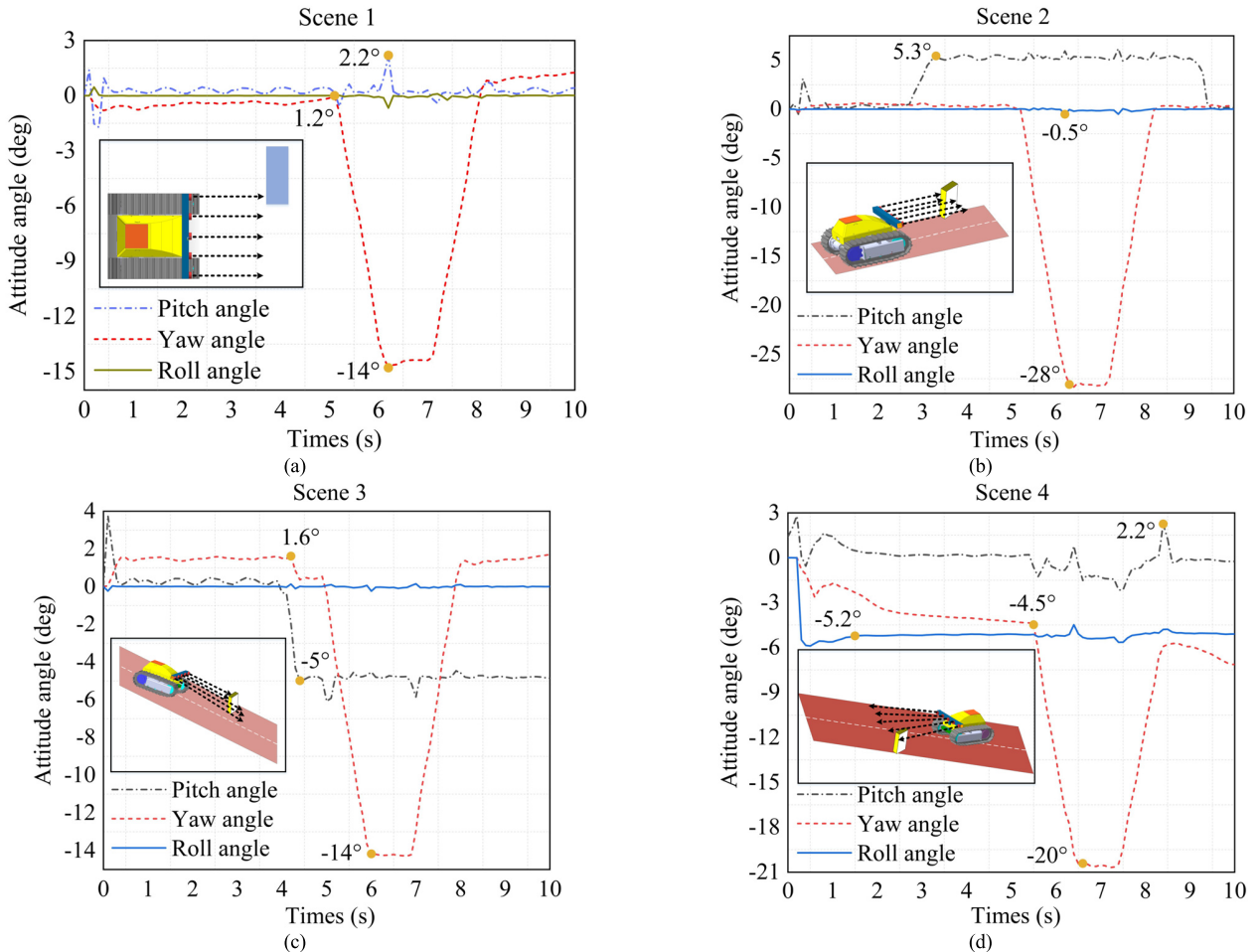


Fig. 10. Schematic diagram of the three-axis attitude angle in four typical obstacle avoidance scenarios during training (a)(b)(c)(d). (a) Obstacle avoidance condition of the unmanned vehicle on the flat road. (b) Obstacle avoidance condition of the unmanned vehicle uphill. (c) Obstacle avoidance condition of the unmanned vehicle downhill. (d) Obstacle avoidance condition of the unmanned vehicle on the longitudinal slope.

vehicle conditions under large-angle maneuvering conditions. The average relative error rate of the deep learning model

established in this study is 15%, which meets the current engineering requirements.

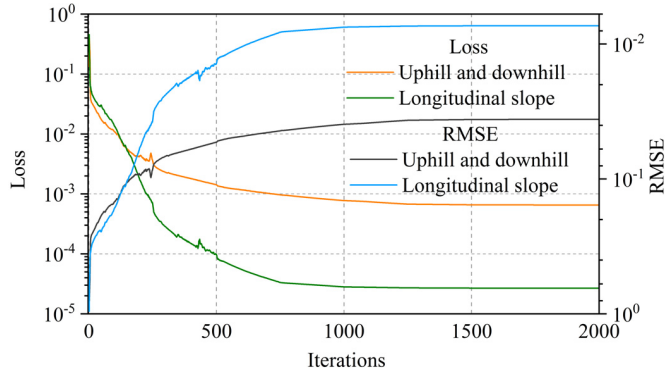


Fig. 11. RMSE and Loss of the Attention-LSTM.

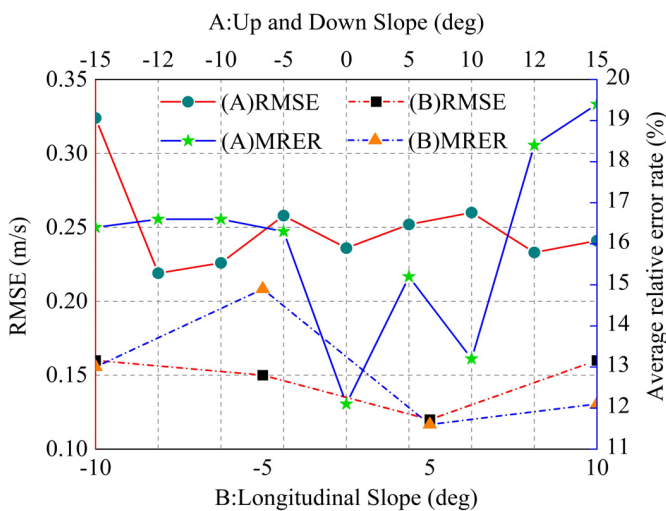


Fig. 12. Root mean square error and average relative error rate diagrams of the proposed model.

TABLE V
PERFORMANCE OF EACH FEATURE EXTRACTION MODEL

Base Model	Average relative error (%)	Loss
GRU	21.77	0.053
LSTM	22.09	0.091
LSTM-CNN	18.97	0.032
RNN	28.12	0.179
BP	34.11	0.237
Proposed model	14.95	0.027

B. Comparison With Other Models

To compare the prediction accuracy of the deep learning algorithms, we used five other popular networks to perform a comprehensive performance evaluation with the model properties proposed in this study. We evaluated the performance of the models using the average relative error rate and loss, as shown in Fig. 13 and Table V.

Based on the violin plot (Fig. 13), the accuracy of our proposed model is far better than other networks, especially the

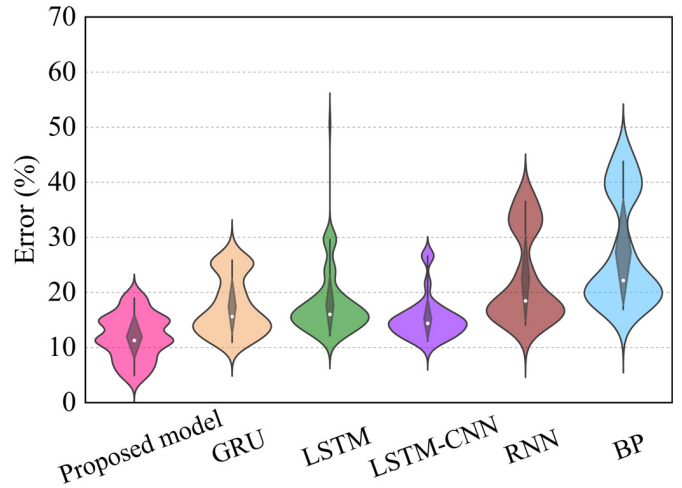


Fig. 13. Violin figure of average relative error for each model.

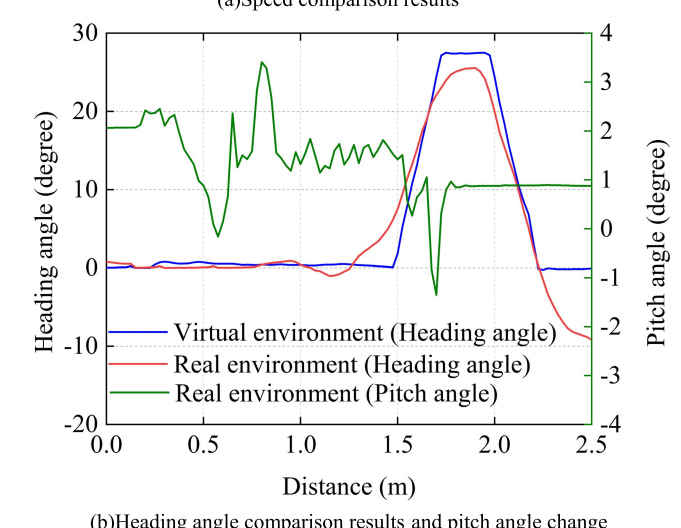
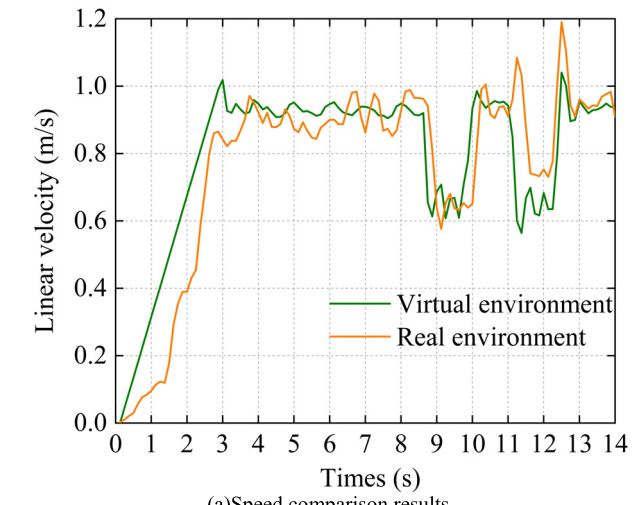


Fig. 14. Preliminary comparison between virtual simulation and real ground experiment (under obstacle avoidance condition on flat road).

BP neural network, whose relative average relative error rate has reached 34.11% with relatively low accuracy. The average

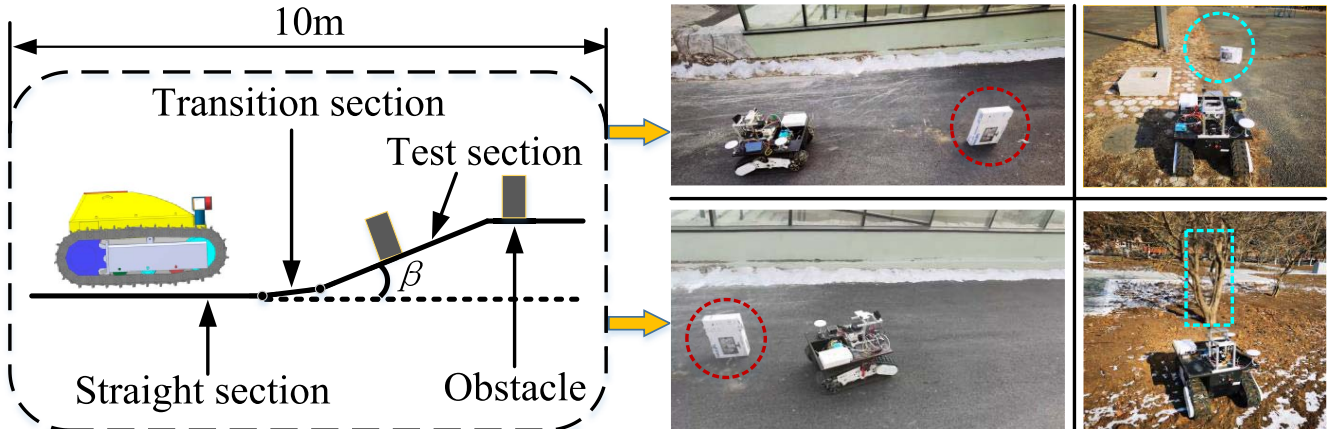


Fig. 15. Obstacle avoidance experiment of driverless vehicle in field environment (the left figure is the environmental diagram, and the right figure is the real environment diagram).

relative error rate of LSTM, RNN, and GRU neural networks has exceeded 20%. Although the average relative error rate of the LSTM-CNN neural network is 18.97%, its error value is more dispersed than the model used in this study. Based on the comparison results, the model used in this study has better accuracy and reliability.

In terms of loss, our model shows a lower loss value than that of other models, as shown in Table V. Clearly, our model is superior to other models in terms of loss.

C. Preliminary Comparison Between Virtual Simulation and Ground Experiment

We conducted simulation and preliminary ground experiments to validate the flat road obstacle avoidance conditions and verify the accuracy of the proposed method. Under the conditions of the exact obstacle locations and sizes in the virtual and natural environments, we used the method proposed in this study to predict the control results of the crawler-type intelligent transport vehicle separately and compared the simulation results with the actual ground experiment results.

Fig. 14 compares the control results after starting the unmanned vehicle under the flat road obstacle avoidance condition. Based on Fig. 14(a), in the natural environment, the speed gradually reaches a stable state after the unmanned vehicle starts. The starting speed differs from that in the natural environment since the unmanned vehicle starts at a constant acceleration in the virtual environment. We selected the unmanned vehicle's speed data when it reached the steady state and calculated the error. The average relative error rate of the centroid speed of the unmanned vehicle in the virtual and real environments is 6.5%, which meets the requirements of this study.

Fig. 14(b) shows the comparison of the heading angle of the unmanned vehicle after startup. Considering the relative turbulence of the ground environment (see the actual pitch angle in Fig. 14(b)), control errors, and other factors, the heading angle error meets the engineering requirements. Based on the figure, the maximum heading angle error of the unmanned vehicle in virtual and real environments is 2° .

The comparison and analysis of the experimental results of the virtual and real environments prove that the method proposed in this study has a good prediction effect and high stability and can be used for the next slope obstacle avoidance experiment.

D. Real World Tests

To verify the accuracy of the method proposed in this study, we conducted field experiments with large slopes for the proposed slope obstacle avoidance conditions. The following is our strategy for deploying work in the actual field environment.

First, we carried out the field ground layout. Fig. 15 shows the test ramp. The test and ramp section lengths must not be less than 8 and 5 m, respectively. There are transition sections in front and behind the test section, and the flat and straight section in front of the slope must not be less than 3 m. According to the engineering requirements, the crawler-type intelligent transport vehicle stops on the straight road section close to the ramp area; after starting and gradually driving into the climbing road, it needs to avoid the obstacles ahead and complete the body back at an appropriate speed. The road is an asphalt pavement with a dry, solid surface and uniform slope. Then, we arranged objects such as foam boxes and masonry as obstacles on the non-structural gradient pavement. Natural obstacles, such as rough stones, were also on the pavement.

We evaluated the success rate of obstacle avoidance by recording unmanned vehicles' driving trajectory and IMU data in the test section (obstacle avoidance completed on 71/72) to demonstrate the effectiveness and feasibility of the method in a natural field environment. The experiment is successful if the unmanned vehicle avoids obstacles and does not lose stability during driving. In this experiment, IMU adopted the northeast sky coordinate system (i.e., y -axis-pointing north, z -axis-pointing skyward, x -axis-pointing eastward). For easier understanding, we transformed the coordinate system accordingly.

Scenario 1: Scenario 1 is the climbing condition of unmanned vehicles, such as in case 4 (see Table I).

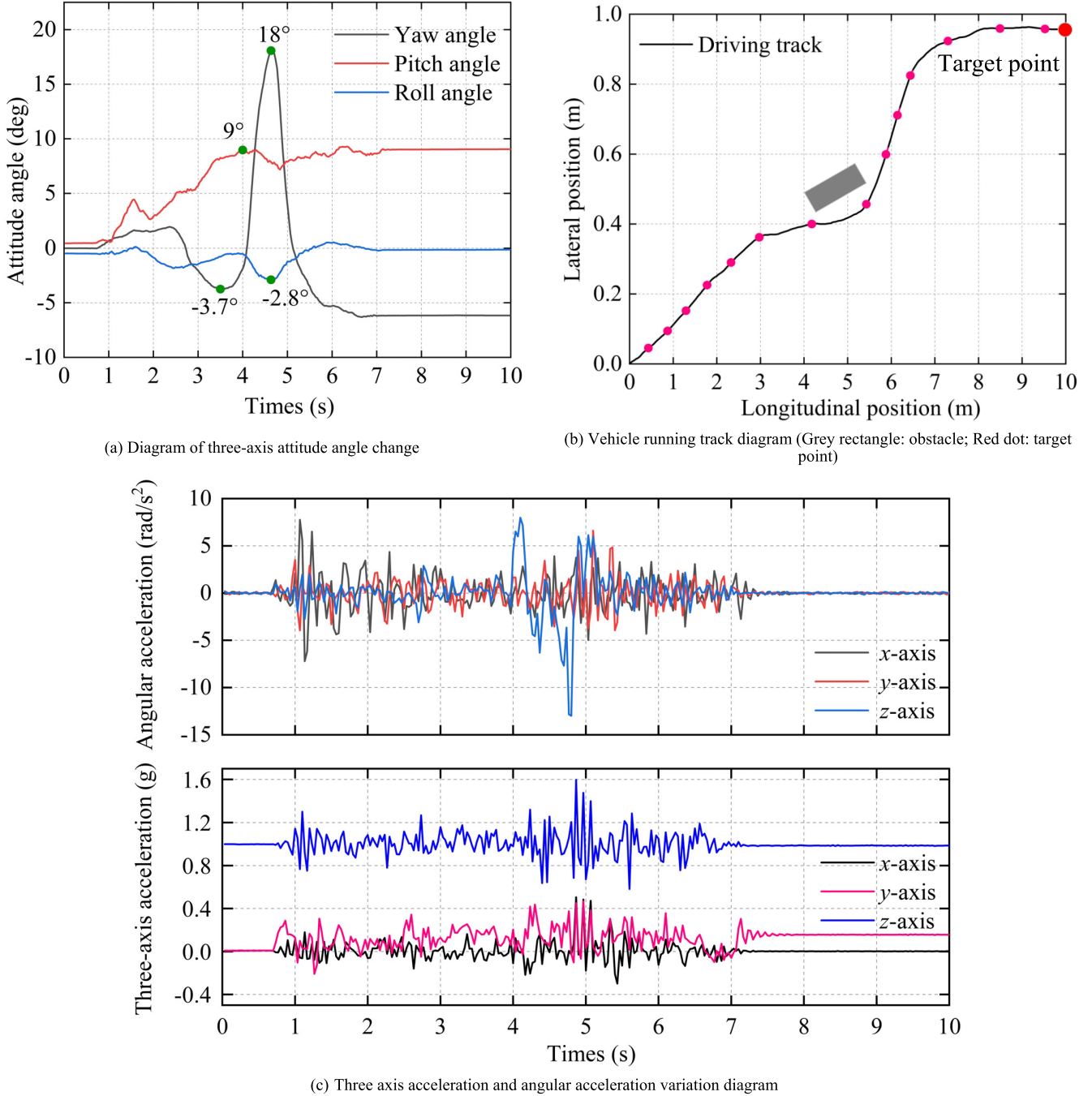


Fig. 16. Experimental result diagram of Scenario 1 (climbing condition).

The variation of the three-axis motion attitude angle of the unmanned vehicle is shown in Fig. 16(a). Based on this figure, the unmanned vehicle performs obstacle avoidance by climbing a 9° slope and decreasing its speed to the left to avoid the obstacle by 21.7°. The driving path and obstacles of the unmanned vehicle are shown in Fig. 16(b), in which the unmanned vehicle successfully plans a safe obstacle avoidance path and steers to avoid obstacles at the 4 s. The three-axis attitude angular acceleration and three-axis acceleration of the unmanned vehicle during driving are shown in Fig. 16(c). From Table VI, the unmanned vehicle's maximum yaw angle

acceleration during obstacle avoidance is -5 rad/s^2 , and the maximum lateral acceleration is 0.5 g . The results show that the stability index of an unmanned vehicle in the obstacle avoidance process is less than the critical value of instability. Our proposed method makes the obstacle avoidance process more efficient and stable.

Scenario 2: Scenario 2 is when the unmanned vehicle performs a downhill working condition, similar to case 14 (see Table I).

The variation of the three-axis motion attitude angle of the unmanned vehicle is shown in Fig. 17(a). Based on this figure,

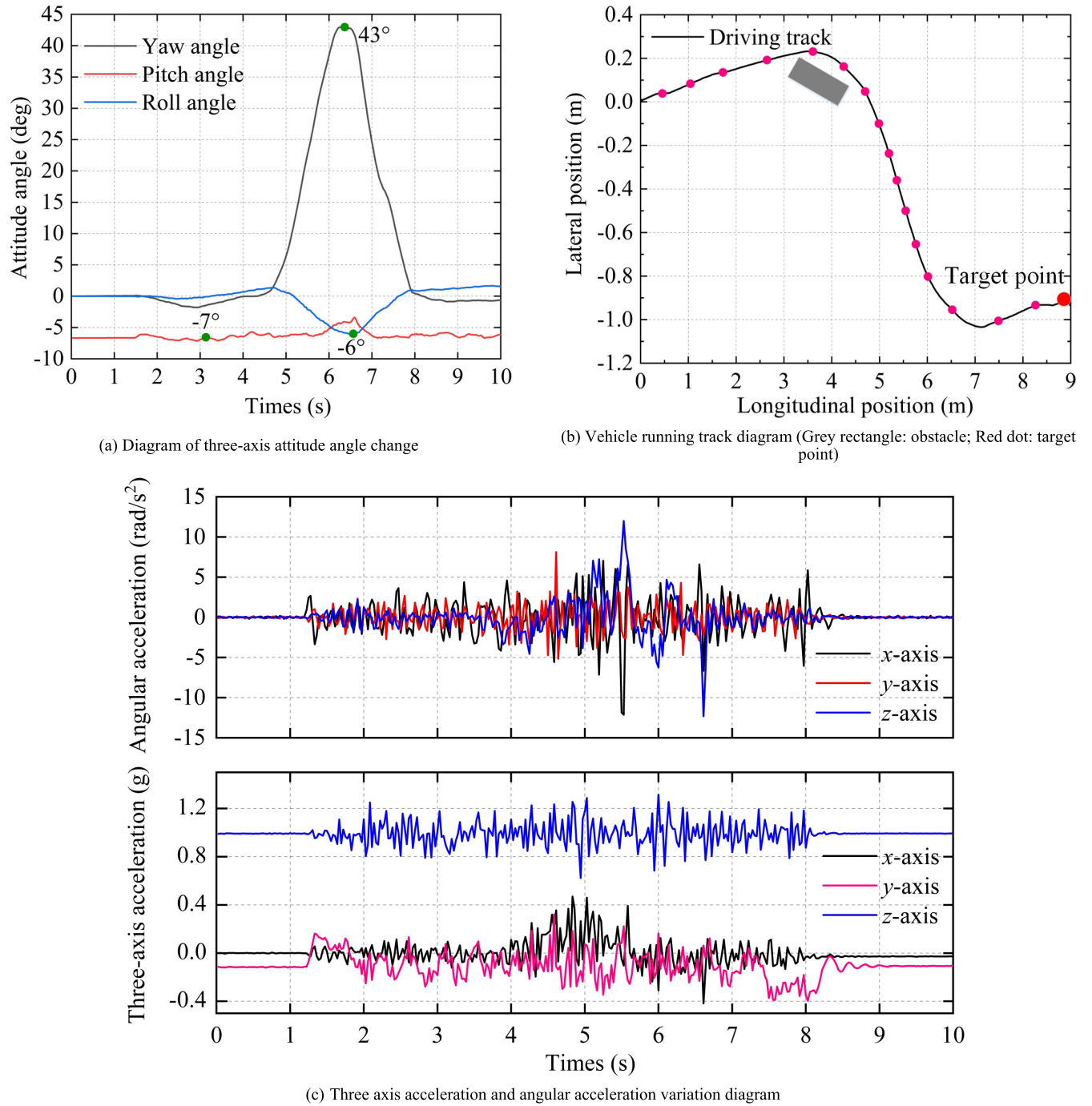


Fig. 17. Experimental result diagram of Scenario 3 (longitudinal slope condition).

the unmanned vehicle is descending and performing obstacle avoidance in a 7° slope. In addition, to avoid obstacles, it slowly slowed down and turned 43° to the left. The travel path and obstacles of the unmanned vehicle are shown in Fig. 17(b). From this figure, the unmanned vehicle successfully plans a safe obstacle avoidance path and makes a steering avoidance at 4.5 s. The three-axis attitude angular acceleration and three-axis acceleration of the unmanned vehicle during travel are shown in Fig. 17(c). According to Table VI, the maximum yaw angular acceleration is -12 rad/s² when the unmanned vehicle avoids obstacles, and the maximum lateral

acceleration is 0.47 g. The results show that the stability index in the obstacle avoidance process is less than the critical instability value, and the obstacle avoidance process of the unmanned vehicle is more efficient and stable based on our proposed method.

Scenario 3: Scenario 3 is when the unmanned vehicle performs a longitudinal slope condition, similar to case 15 (see Table I).

The variation of the three-axis motion attitude angle of the unmanned vehicle is shown in Fig. 18(a). Based on this figure, the unmanned vehicle performed the obstacle avoidance

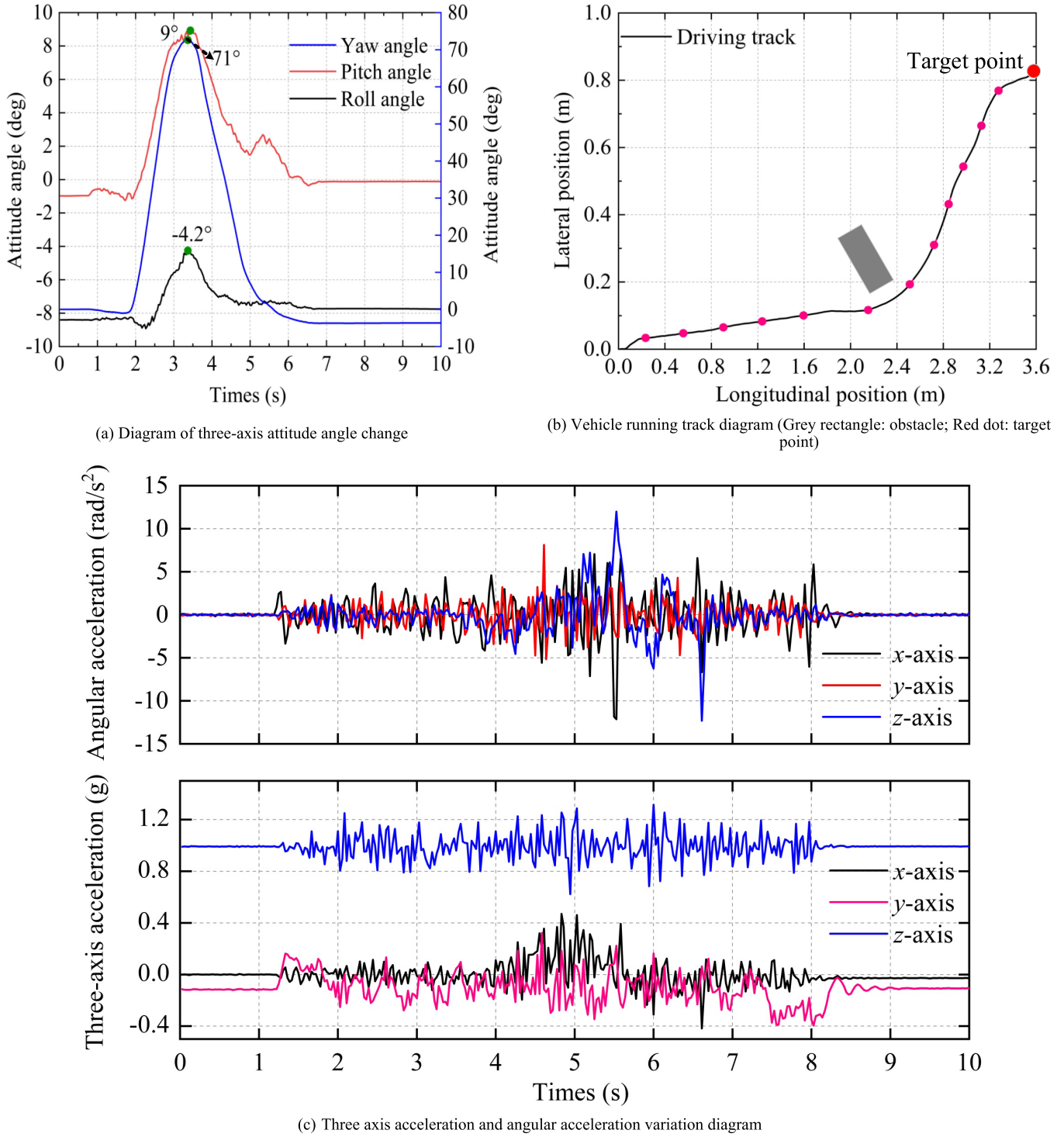


Fig. 18. Experimental result diagram of Scenario 2 (downhill condition).

condition on the longitudinal slope (the slope is -6°). The unmanned vehicle reduced the speed and turned to the left at 71° to avoid the obstacle (for ease of understanding, the right-side ordinate is the heading angle). The driving path and obstacles of the unmanned vehicle are shown in Fig. 18(b). From this figure, the unmanned vehicle successfully plans a safe obstacle avoidance path and makes a turn for obstacle avoidance at 4 s. The three-axis attitude angular acceleration

and three-axis acceleration of the unmanned vehicle during travel are shown in Fig. 18(c). According to Table VI, the maximum yaw angular acceleration of the unmanned vehicle during obstacle avoidance is -12.1 rad/s^2 , the maximum roll angular acceleration is 11.8 rad/s^2 , and the maximum lateral acceleration is 0.56 g . The results show that the stability index in the obstacle avoidance process is less than the critical value of instability. Based on our proposed method, the obstacle

TABLE VI
TRIAXIAL ANGULAR ACCELERATION AND ACCELERATION OF VEHICLE

Evaluating indicator	Slope angle (angle)	Around the x-axis (rad/s ²)	Around the y-axis(rad/s ²)	Around the z-axis (rad/s ²)	x-axis (g)	y-axis (g)	z-axis (g)	DSE (max)
Experiment 1	9	7.76	6.61	7.98	0.50	0.47	1.60	3.11
Experiment 2	-7	-12.13	8.11	-12.32	0.47	-0.39	1.32	4.29
Experiment 3	-6	-12.10	11.87	-15.38	0.70	0.59	1.47	5.63

avoidance process of unmanned vehicle is more efficient and stable.

As shown in Table VI, the maximum dynamic stability index values of the three large-slope ground experiments are less than the critical value of instability required by the project, and no instability occurs in unmanned vehicles.

According to engineering requirements, we set the initial speed of the unmanned vehicle to 0.9 m/s. We conducted 72 vehicle obstacle avoidance experiments, and the success rate of the experiment was 98.7%. Note that our outdoor environment is conducted in rainy, snowy, and cold weather with relatively poor road conditions, which is very different from the training environment, bringing more difficulties to the deep learning algorithm and stable obstacle avoidance. In addition, it demonstrated the generalization ability and feasibility of our proposed model for unknown environments.

VI. CONCLUSION AND PROSPECTS

Crawler-type intelligent transportation vehicles are prone to safety accidents such as collisions and rollovers when driving autonomously, which seriously affects the application of automated transportation vehicles in non-structural environments.

To address the above issues:

(1) In this study, combined with the recognition methods of human drivers for obstacles in the field, the obstacles are identified and classified according to their characteristics and spatial position relationship. This method effectively reduces the obstacle identification workload and helps plan the optimal obstacle avoidance path for vehicles.

(2) In this study, according to the characteristics of the non-structural environment, the driving characteristics of crawler-type vehicles in non-structural environments are studied, and a stability evaluation index of crawler-type intelligent transportation vehicles based on non-structural roads is proposed.

(3) A stable obstacle avoidance control strategy is designed based on the evaluation index. Based on the attention LSTM network, this strategy learns human drivers' driving habits, enabling vehicles to complete stable obstacle avoidance behavior when encountering obstacles independently.

After a large number of actual vehicle tests, it is verified that the stability index proposed by us has a more reasonable parameter weight, which can better guide the development of a control algorithm for crawler-type intelligent transport vehicles; The obstacle avoidance control strategy proposed by us can ensure the driving stability and safety of vehicles in the unstructured slope environment.

In future work, we will further study the dynamic obstacle avoidance problem in a non-structural environment to improve the vehicle's autonomous obstacle avoidance technology.

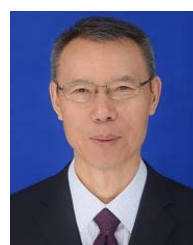
REFERENCES

- [1] Y. Sun, L. Xu, B. Jing, X. Chai, and Y. Li, "Development of a four-point adjustable lifting crawler chassis and experiments in a combine harvester," *Comput. Electron. Agricult.*, vol. 173, Jun. 2020, Art. no. 105416.
- [2] G. Lee, K. Ogata, and C. Li, "Autonomous shape-variable crawler: One-dimensional displacement coordination for constant upper frame posture," *IEEE Trans. Intell. Transp. Syst.*, vol. 23, no. 9, pp. 14968–14977, Dec. 2021.
- [3] N. Wang and Z. Deng, "Finite-time fault estimator based fault-tolerance control for a surface vehicle with input saturations," *IEEE Trans. Ind. Informat.*, vol. 16, no. 2, pp. 1172–1181, Feb. 2020.
- [4] Y. Huang et al., "A motion planning and tracking framework for autonomous vehicles based on artificial potential field elaborated resistance network approach," *IEEE Trans. Ind. Electron.*, vol. 67, no. 2, pp. 1376–1386, Feb. 2020.
- [5] C. You and P. Tsotras, "High-speed cornering for autonomous off-road rally racing," *IEEE Trans. Control Syst. Technol.*, vol. 29, no. 2, pp. 485–501, Mar. 2021.
- [6] T. Chen, L. Chen, Y. Cai, and X. Xu, "Robust sideslip angle observer with regional stability constraint for an uncertain singular intelligent vehicle system," *IET Control Theory Appl.*, vol. 12, no. 13, pp. 1802–1811, Sep. 2018.
- [7] X. Hu, L. Chen, B. Tang, D. Cao, and H. Hee, "Dynamic path planning for autonomous driving on various roads with avoidance of static and moving obstacles," *Mech. Syst. Signal Process.*, vol. 100, pp. 482–500, Feb. 2018.
- [8] Y. Tang et al., "Vision-aided multi-UAV autonomous flocking in GPS-denied environment," *IEEE Trans. Ind. Electron.*, vol. 66, no. 1, pp. 616–626, Jan. 2019.
- [9] P. K. Mohanty and H. S. Dewang, "A smart path planner for wheeled mobile robots using adaptive particle swarm optimization," *J. Brazilian Soc. Mech. Sci. Eng.*, vol. 43, no. 2, Jan. 2021.
- [10] H. Yang, Q. Li, Z. Zuo, and H. Zhao, "Event-triggered model predictive control for multi-vehicle systems with collision avoidance and obstacle avoidance," *Int. J. Robust Nonlinear Control*, vol. 31, no. 11, pp. 5476–5494, Apr. 2021.
- [11] Y.-C. Chang et al., "Interpretable fuzzy logic control for multirobot coordination in a cluttered environment," *IEEE Trans. Fuzzy Syst.*, vol. 29, no. 12, pp. 3676–3685, Dec. 2021.
- [12] C. Badue et al., "Self-driving cars: A survey," *Exp. Syst. Appl.*, vol. 165, Mar. 2021, Art. no. 113816.
- [13] B. Guo, N. Guo, and Z. Cen, "Obstacle avoidance with dynamic avoidance risk region for mobile robots in dynamic environments," *IEEE Robot. Autom. Lett.*, vol. 7, no. 3, pp. 5850–5857, Jul. 2022.
- [14] T. Xu, S. Zhang, Z. Jiang, Z. Liu, and H. Cheng, "Collision avoidance of high-speed obstacles for mobile robots via maximum-speed aware velocity obstacle method," *IEEE Access*, vol. 8, pp. 138493–138507, 2020.
- [15] X. Zhou, X. Yu, Y. Zhang, Y. Luo, and X. Peng, "Trajectory planning and tracking strategy applied to an unmanned ground vehicle in the presence of obstacles," *IEEE Trans. Autom. Sci. Eng.*, vol. 18, no. 4, pp. 1575–1589, Oct. 2021.
- [16] S. Li, Z. Li, Z. Yu, B. Zhang, and N. Zhang, "Dynamic trajectory planning and tracking for autonomous vehicle with obstacle avoidance based on model predictive control," *IEEE Access*, vol. 7, pp. 132074–132086, 2019.

- [17] M. Xu et al., "Crowd behavior simulation with emotional contagion in unexpected multihazard situations," *IEEE Trans. Syst., Man, Cybern. Syst.*, vol. 51, no. 3, pp. 1567–1581, Mar. 2021.
- [18] J. Ji, A. Khajepour, W. W. Melek, and Y. Huang, "Path planning and tracking for vehicle collision avoidance based on model predictive control with multiconstraints," *IEEE Trans. Ultrason. Eng.*, vol. 66, no. 2, pp. 952–964, Feb. 2017.
- [19] J. Hu, Y. Hu, C. Lu, J. Gong, and H. Chen, "Integrated path planning for unmanned differential steering vehicles in off-road environment with 3D terrains and obstacles," *IEEE Trans. Intell. Transp. Syst.*, vol. 23, no. 6, pp. 5562–5572, Feb. 2021.
- [20] A. Schaub, D. Baumgartner, and D. Burschka, "Reactive obstacle avoidance for highly maneuverable vehicles based on a two-stage optical flow clustering," *IEEE Trans. Intell. Transp. Syst.*, vol. 18, no. 8, pp. 2137–2152, Aug. 2017.
- [21] S. Gim, S. Lee, and L. Adouane, "Safe and efficient lane change maneuver for obstacle avoidance inspired from human driving pattern," *IEEE Trans. Intell. Transp. Syst.*, vol. 23, no. 3, pp. 2155–2169, Mar. 2022.
- [22] G. Li et al., "Risk assessment based collision avoidance decision-making for autonomous vehicles in multi-scenarios," *Transp. Res. C, Emerg. Technol.*, vol. 122, Jan. 2021, Art. no. 102820.
- [23] X. Li, Z. Sun, D. Cao, D. Liu, and H. He, "Development of a new integrated local trajectory planning and tracking control framework for autonomous ground vehicles," *Mech. Syst. Signal Process.*, vol. 87, pp. 118–137, Mar. 2017.
- [24] J. Shi et al., "Prediction of brake pedal aperture for automatic wheel loader based on deep learning," *Autom. Construction*, vol. 119, Nov. 2020, Art. no. 103313.
- [25] J. Chen, C. Zhang, J. Luo, J. Xie, and Y. Wan, "Driving maneuvers prediction based autonomous driving control by deep Monte Carlo tree search," *IEEE Trans. Veh. Technol.*, vol. 69, no. 7, pp. 7146–7158, Jul. 2020.
- [26] T. Sun, Z. Gao, F. Gao, T. Zhang, S. Chen, and K. Zhao, "A brain-inspired decision-making linear neural network and its application in automatic drive," *Sensors*, vol. 21, no. 3, p. 794, Jan. 2021.
- [27] S. Liang, C. Chen, and G. Zou, "Intelligent driving system of robot based on computer vision and neural network algorithm," *J. Intell. Fuzzy Syst.*, vol. 38, no. 6, pp. 7279–7290, Jun. 2020.
- [28] Y. Liu, Y. Yixuan, and M. Liu, "Ground-aware monocular 3D object detection for autonomous driving," *IEEE Robot. Autom. Lett.*, vol. 6, no. 2, pp. 919–926, Apr. 2021.
- [29] M. Aladem and S. A. Rawashdeh, "A single-stream segmentation and depth prediction CNN for autonomous driving," *IEEE Intell. Syst.*, vol. 36, no. 4, pp. 79–85, Jul. 2021.
- [30] X. Huang, J. Sun, and J. Sun, "A car-following model considering asymmetric driving behavior based on long short-term memory neural networks," *Transp. Res. C, Emerg. Technol.*, vol. 95, pp. 346–362, Oct. 2018.
- [31] Y. Zhang, J. Li, Y. Guo, C. Xu, J. Bao, and Y. Song, "Vehicle driving behavior recognition based on multi-view convolutional neural network with joint data augmentation," *IEEE Trans. Veh. Technol.*, vol. 68, no. 5, pp. 4223–4234, May 2019.
- [32] L. Wu and Y. Wu, "Simulation of transmission system of crawler self-propelled rotary tiller based on deep learning," *Comput. Intell. Neurosci.*, vol. 2022, Jul. 2022, Art. no. 6078223.
- [33] E. Takane, K. Tadakuma, M. Watanabe, M. Konyo, and S. Tadokoro, "Design and control method of a planar omnidirectional crawler mechanism," *J. Mech. Design*, vol. 144, no. 1, Jan. 2022, Art. no. 013302.
- [34] M. Kormanek and J. Dvořák, "Ground pressure changes caused by MHT 8002HV crawler harvester chassis," *Croatian J. Forest Eng.*, vol. 42, no. 2, pp. 201–211, Mar. 2021.
- [35] Z. Tang, B. Zhang, X. Liu, H. Ren, X. Li, and Y. Li, "Structural model and bundling capacity of crawler picking and baling machine for straw wasted in field," *Comput. Electron. Agricult.*, vol. 175, Aug. 2020, Art. no. 105622.
- [36] V. Alakshendra and S. S. Chiddarwar, "Adaptive robust control of mecanum-wheeled mobile robot with uncertainties," *Nonlinear Dyn.*, vol. 87, no. 4, pp. 2147–2169, Nov. 2016.
- [37] F. Galasso, D. Lodi Rizzini, F. Oleari, and S. Caselli, "Efficient calibration of four wheel industrial AGVs," *Robot. Comput.-Integr. Manuf.*, vol. 57, pp. 116–128, Jun. 2019.
- [38] Z. Li, J. Deng, R. Lu, Y. Xu, J. Bai, and C.-Y. Su, "Trajectory-tracking control of mobile robot systems incorporating neural-dynamic optimized model predictive approach," *IEEE Trans. Syst., Man, Cybern., Syst.*, vol. 46, no. 6, pp. 740–749, Jun. 2016.
- [39] Z. Yao, G. Wang, X. Li, J. Qu, Y. Zhang, and Y. Yang, "Dynamic simulation for the rollover stability performances of articulated vehicles," *Proc. Inst. Mech. Eng., D, J. Automobile Eng.*, vol. 228, no. 7, pp. 771–783, Jun. 2014.
- [40] M. Ataei, A. Khajepour, and S. Jeon, "Model predictive control for integrated lateral stability, traction/braking control, and rollover prevention of electric vehicles," *Vehicle Syst. Dyn.*, vol. 58, no. 1, pp. 49–73, Mar. 2019.
- [41] M. Li, F. Lu, H. Zhang, and J. Chen, "Predicting future locations of moving objects with deep fuzzy-LSTM networks," *Transportmetrica A, Transp. Sci.*, vol. 16, no. 1, pp. 119–136, Dec. 2018.
- [42] J. Zhao, F. Deng, Y. Cai, and J. Chen, "Long short-term memory–fully connected (LSTM-FC) neural network for PM2.5 concentration prediction," *Chemosphere*, vol. 220, pp. 486–492, Apr. 2019.
- [43] Y. Yu, X. Si, C. Hu, and Z. Jianxun, "A review of recurrent neural networks: LSTM cells and network architectures," *Neural Comput.*, vol. 31, no. 7, pp. 1235–1270, 2019.
- [44] X. Li, L. Zhang, Z. Wang, and P. Dong, "Remaining useful life prediction for lithium-ion batteries based on a hybrid model combining the long short-term memory and Elman neural networks," *J. Energy Storage*, vol. 21, pp. 510–518, Feb. 2019.
- [45] X. Shu, J. Tang, G.-J. Qi, W. Liu, and J. Yang, "Hierarchical long short-term concurrent memory for human interaction recognition," *IEEE Trans. Pattern Anal. Mach. Intell.*, vol. 43, no. 3, pp. 1110–1118, Mar. 2021.
- [46] Z. S. Khozani, F. B. Banadkooki, M. Ehteram, A. N. Ahmed, and A. El-Shafie, "Combining autoregressive integrated moving average with long short-term memory neural network and optimisation algorithms for predicting ground water level," *J. Cleaner Prod.*, vol. 348, May 2022, Art. no. 131224.
- [47] V. Nourani, E. Sharghi, N. Behfar, and Y. Zhang, "Multi-step-ahead solar irradiance modeling employing multi-frequency deep learning models and climatic data," *Appl. Energy*, vol. 315, Jun. 2022, Art. no. 119069.
- [48] A. Mahmoodzadeh et al., "Machine learning techniques to predict rock strength parameters," *Rock Mech. Rock Eng.*, vol. 55, no. 3, pp. 1721–1741, Mar. 2022.
- [49] J. Gao, H. Wang, and H. Shen, "Task failure prediction in cloud data centers using deep learning," *IEEE Trans. Services Comput.*, vol. 15, no. 3, pp. 1411–1422, May 2022.
- [50] J. Tang, X. Shu, R. Yan, and L. Zhang, "Coherence constrained graph LSTM for group activity recognition," *Trans. Pattern Anal. Mach. Intell.*, vol. 44, no. 2, pp. 636–647, 2022.
- [51] R. W. Liu, M. Liang, J. Nie, W. Y. B. Lim, Y. Zhang, and M. Guizani, "Deep learning-powered vessel trajectory prediction for improving smart traffic services in maritime Internet of Things," *IEEE Trans. Netw. Sci. Eng.*, vol. 9, no. 5, pp. 3080–3094, Sep. 2022.
- [52] T. Chen, L. Lin, R. Chen, X. Hui, and H. Wu, "Knowledge-guided multi-label few-shot learning for general image recognition," *IEEE Trans. Pattern Anal. Mach. Intell.*, vol. 44, no. 3, pp. 1371–1384, Mar. 2022.



Yitian Wang received the B.S. degree in mechanical design, manufacturing and automation from the Changchun University of Science and Technology, Changchun, China, in 2016. He is currently pursuing the Ph.D. degree with the College of Instrumentation and Electrical Engineering, Jilin University. His research interests include path planning and pose estimation.



Jun Lin is currently an Academician with the Chinese Academy of Engineering, Beijing, China. He also serves as the Director of the National Geophysical Exploration Equipment Engineering Research Center, Jilin University, Changchun, China. His research interests include geophysical exploration theory, technologies, and equipment.



Liu Zhang was born in Bengbu, Anhui, China, in 1978. He received the Ph.D. degree from the Harbin Institute of Technology in 2007. He is currently a Professor with the College of Instrumentation and Electrical Engineering, Jilin University. His research interests include aerospace optical remote sensing system design, simulation and application technology, and star sensor technology.



Yuehan Qi is currently pursuing the bachelor's degree (Hons.) in computing with Queen's University, Kingston, ON, Canada. Her current research interests include machine learning and computer vision.



Tianhao Wang (Member, IEEE) received the B.S. degree in electrical engineering and the Ph.D. degree in vehicle engineering from Jilin University, Changchun, Jilin, China, in 2010 and 2016, respectively. From 2016 to 2019, he was a Post-Doctoral Researcher with the Department of Science and Technology of Instrument, Jilin University. He is currently an Assistant Professor with the College of Instrumentation and Electrical Engineering, Jilin University. His research interests include numerical and experimental studies of crosstalk in complex cable bundles, with a particular emphasis on considering parameter variability using efficient statistical approaches.



Guanyu Zhang received the M.S. and Ph.D. degrees in mechanical engineering from Jilin University in 2015. He is currently an Associate Professor with the Department of Instrument Science and Electrical Engineering, Jilin University. His research interests include mechatronics system design and artificial intelligence control technology research.



Hao Xu received the B.S. degree from the Changchun University of Technology and the M.S. degree from Jilin University, Changchun, China, where he is currently pursuing the Ph.D. degree with the School of Instrument Science and Electrical Engineering. His research interests include path planning of intelligent robots.



Yang Liu received the Ph.D. degree from Jilin University in 2020. He is currently working as an Assistant Research Fellow with Jilin University. His research interests include stereo vision, 3D reconstruction, texture filtering, and SLAM.